



**Discover Generics**

Cost-Effective CT & MRI Contrast Agents

**FRESENIUS  
KABI**

[WATCH VIDEO](#)

**AJNR**








This information is current as  
of June 17, 2025.

**CT Texture Analysis of Cervical Lymph  
Nodes on Contrast-Enhanced [ $^{18}\text{F}$ ]  
FDG-PET/CT Images to Differentiate Nodal  
Metastases from Reactive Lymphadenopathy  
in HIV-Positive Patients with Head and Neck  
Squamous Cell Carcinoma**

H. Kuno, N. Garg, M.M. Qureshi, M.N. Chapman, B. Li,  
S.K. Meibom, M.T. Truong, K. Takumi and O. Sakai

*AJNR Am J Neuroradiol* published online 21 February 2019  
<http://www.ajnr.org/content/early/2019/02/21/ajnr.A5974>

# CT Texture Analysis of Cervical Lymph Nodes on Contrast-Enhanced [<sup>18</sup>F] FDG-PET/CT Images to Differentiate Nodal Metastases from Reactive Lymphadenopathy in HIV-Positive Patients with Head and Neck Squamous Cell Carcinoma

 H. Kuno,  N. Garg,  M.M. Qureshi,  M.N. Chapman,  B. Li,  S.K. Meibom,  M.T. Truong,  K. Takumi, and  O. Sakai



## ABSTRACT

**BACKGROUND AND PURPOSE:** Differentiating nodal metastases from reactive adenopathy in HIV-infected patients with [<sup>18</sup>F] FDG-PET/CT can be challenging because lymph nodes in HIV-positive patients often show increased [<sup>18</sup>F] FDG uptake. The purpose of this study was to assess CT textural analysis characteristics of HIV-positive and HIV-negative lymph nodes on [<sup>18</sup>F] FDG-PET/CT to differentiate nodal metastases from disease-specific nodal reactivity.

**MATERIALS AND METHODS:** Nine HIV-positive patients with head and neck squamous cell carcinoma (7 men, 2 women; 29–62 years of age; median age, 48 years) with 22 lymph nodes ( $\geq 1$  cm) who underwent contrast-enhanced CT with [<sup>18</sup>F] FDG-PET followed by pathologic evaluation of cervical lymph nodes were retrospectively reviewed. Twenty-six HIV-negative patients with head and neck squamous cell carcinoma with 61 lymph nodes were evaluated as a control group. Each lymph node was manually segmented, and an in-house-developed Matlab-based texture analysis program extracted 41 texture features from each segmented volume. A mixed linear regression model was used to compare the pathologically proved malignant lymph nodes with benign nodes in the 2 enrolled groups.

**RESULTS:** Thirteen (59%) lymph nodes in the HIV-positive group and 22 (36%) lymph nodes in the HIV-negative control group were confirmed as positive for metastases. There were 7 histogram features ( $P = .017$ – $0.032$ ), 3 gray-level co-occurrence features ( $P = .009$ – $.025$ ), and 9 gray-level run-length features ( $P < .001$ – $.033$ ) that demonstrated a significant difference in HIV-positive patients with either benign or malignant lymph nodes.

**CONCLUSIONS:** CT texture analysis may be useful as a noninvasive method of obtaining additional quantitative information to differentiate nodal metastases from disease-specific nodal reactivity in HIV-positive patients with head and neck squamous cell carcinoma.

**ABBREVIATIONS:** AUC = area under receiver operating characteristic curve; HNSCC = head and neck squamous cell carcinoma; GLCM = gray-level co-occurrence matrix; GLGM = gray-level gradient matrix; GLN = gray-level nonuniformity; GLRL = gray-level run-length; HGRE = high gray-level run emphasis; LGRE = low gray-level run emphasis; LRE = long-run emphasis; LRHGE = long-run high gray-level emphasis; max = maximum; RLN = run-length nonuniformity; RP = run percentage; SRE = short-run emphasis; SRLGE = short-run low gray-level emphasis; SUV = standard uptake value

Although patients with HIV have increased life expectancies through the introduction of highly active antiretroviral therapy,<sup>1</sup> there remains significant cancer-specific mortality in these

patients.<sup>2,3</sup> Many of these patients are now acquiring malignancies that had previously not been associated with HIV or AIDS.<sup>4,5</sup> The HIV-positive population is at an increased risk of head and neck squamous cell carcinoma (HNSCC) compared with the general population,<sup>6,7</sup> and HNSCC is an increasingly common disease among individuals with HIV.<sup>8</sup> HIV-positive HNSCCs have a more aggressive profile that leads to poorer patient outcomes,<sup>9</sup> and HIV-positive patients have a concurrent increase in HNSCC-related mortality.<sup>3,4,10</sup>

CT is the initial imaging technique for the diagnosis and staging of HNSCC below the hard palate at many institutions. However, HIV-positive patients often have diffuse bilateral lymph node enlargement consistent with AIDS-associated reactive adenopathy, cystic lesions, necrosis, or infections,<sup>11,12</sup> and CT is sometimes limited for nodal staging. The introduction of [<sup>18</sup>F] FDG-PET/CT has enabled the metabolic assessment of lymph

Received January 26, 2018; accepted after revision January 5, 2019.

From the Departments of Radiology (H.K., N.G., M.M.Q., M.N.C., B.L., S.K.M., M.T.T., K.T., O.S.), Radiation Oncology (M.M.Q., M.T.T., O.S.), and Otolaryngology–Head and Neck Surgery (O.S.), Boston Medical Center, Boston University School of Medicine, Boston, Massachusetts; Department of Diagnostic Radiology (H.K.), National Cancer Center Hospital East, Kashiwa, Chiba, Japan; and Department of Radiology (K.T.), Kagoshima University Graduate School of Medical and Dental Sciences, Kagoshima, Japan.

Please address correspondence to Osamu Sakai, MD, PhD, FACR, Department of Radiology, Boston Medical Center, Boston University School of Medicine, FGH Building, 3rd Floor, 820 Harrison Ave, Boston, MA 02118; e-mail: osamu.sakai@bmc.org



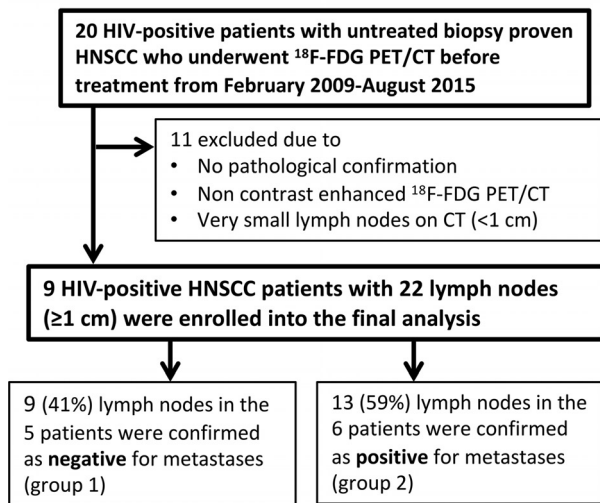
Indicates article with supplemental on-line appendix and tables.



Indicates article with supplemental on-line photo.

<http://dx.doi.org/10.3174/ajnr.A5974>

## • HIV-positive group



## • HIV-negative control group

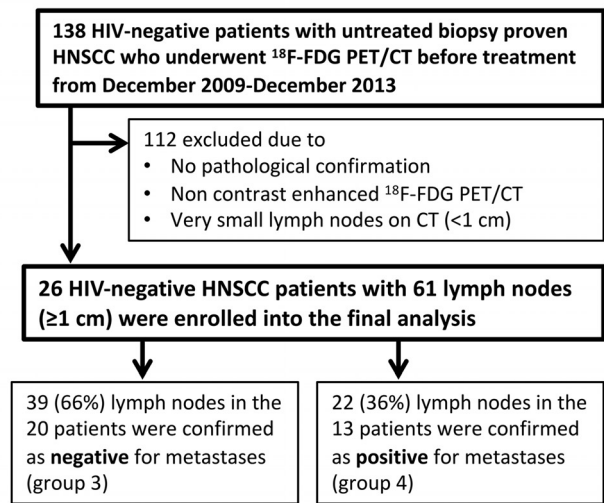


**FIG 1.** Flowchart shows patient selection for the study.

nodes and is widely used for initially staging, restaging, and monitoring therapeutic responses for patients with head and neck squamous cell carcinoma.<sup>13-15</sup> However, lymph nodes in HIV-positive patients often show increased [<sup>18</sup>F] FDG uptake, especially in the setting of high-plasma HIV RNA.<sup>16-18</sup> Activated lymphocytes exhibit increased glucose use, and HIV-positive individuals have a greater accumulation of FDG in their lymph nodes than HIV-negative patients. Both HIV-1 and HNSCC can spread to the primary site of regional deep cervical lymph nodes,<sup>19,20</sup> which makes metastatic determination and management complex.

There is increasing focus on using texture analysis to determine the features of CT images and elicit characteristics that may adequately describe nodal metastases despite the viral adenopathy.<sup>21-23</sup> Image texture analysis analyzes complex visual characteristics on the basis of underlying simpler patterns and then conducts quantitative comparisons of these characteristics between 2 images. Considering that these mathematic textural analyses have helped elucidate nuanced differences in pathology, we hypothesized that CT textural features would have the potential to add additional quantitative information in conjunction with [<sup>18</sup>F] FDG-PET/CT in HIV-positive HNSCC for the evaluation of lymph nodes. In addition, to the best of our knowledge, imaging studies including [<sup>18</sup>F] FDG-PET/CT of HIV-positive patients with head and neck squamous cell carcinoma related to lymph node adenopathy have not been fully explored in the literature. Hence, the purpose of this study was to assess the CT texture-analysis characteristics of HIV-positive and HIV-negative lymph nodes on [<sup>18</sup>F] FDG-PET/CT to differentiate nodal metastases from disease-specific nodal reactivity.

## MATERIALS AND METHODS

### Patients

The institutional review board approved this retrospective study. The requirement to obtain written informed consent was waived. The flowcharts of patient selection for HIV-positive patients and an HIV-negative control group in the study are shown in Fig 1.

### HIV-Positive Patient Group

We retrospectively searched our electronic medical records to identify HIV-positive patients with untreated biopsy-proven HNSCCs who also underwent [<sup>18</sup>F] FDG-PET/CT before treatment between February 2009 and August 2015, and 20 patients were identified in total. Four of the 20 patients were excluded because they received nonsurgical treatment, such as chemoradiotherapy, without biopsy-proved pathologic confirmation of cervical lymph nodes. An additional 7 patients were excluded, 3 of whom were excluded due to non-contrast-enhanced [<sup>18</sup>F] FDG-PET/CT; and 4 patients, due to very small lymph nodes on CT (maximum size, <1 cm) that were difficult to analyze using the texture-analysis program. The remaining 9 patients (7 men, 2 women; 29–62 years of age; median age, 48 years; with 3 oral cavity, 3 oropharynx, 1 larynx, 1 maxillary sinus, and 1 primary unknown lesion) with 22 lymph nodes (maximum size, ≥1 cm) were enrolled in this study.

The electronic medical records were reviewed on all subjects, specifically for the presence of pathologically confirmed cervical lymph node metastasis at first treatment with neck dissection. The dates of the first surgical procedure and patient outcomes such as the presence of metastatic recurrence in a cervical lymph node within 1 year after surgery were also noted.

### HIV-Negative Patient Group for Controls

We also identified HIV-negative patients with untreated biopsy-proved HNSCCs as a control group to investigate how HIV infection affects the texture features and standard uptake values (SUVs) of the nodal metastasis and reactive adenopathy. Between December 2009 and December 2013, one hundred thirty-eight consecutive HIV-negative patients with newly diagnosed primary head and neck squamous cell carcinoma underwent [<sup>18</sup>F] FDG-PET/CT before treatment. Fifty-three of the 138 patients were excluded because they received nonsurgical treatment without pathologic confirmation of cervical lymph nodes. An additional 25 patients were excluded because only non-contrast-enhanced [<sup>18</sup>F] FDG-PET/CT was performed. In addition, 34 patients with

small lymph nodes on CT (maximum size, <1 cm) were also excluded. The remaining 26 patients (17 men, 9 women; 30–86 years of age; median age, 59 years; with 12 oral cavity, 10 oropharynx, 1 hypopharynx, and 3 larynx lesions) with 61 lymph nodes (node size,  $\geq 1$  cm) were enrolled in this study as a control group.

### **PET/CT Imaging Protocol**

For image analysis, the pretreatment PET/CT was used to obtain CT texture analysis and FDG uptake. All [ $^{18}\text{F}$ ] FDG-PET/CT studies were performed on an integrated PET/CT scanner combining PET with a 16-slice multidetector row CT (Discovery STE 16; GE Healthcare, Milwaukee, Wisconsin). Patients were injected with an average of 10.59 mCi of [ $^{18}\text{F}$ ] FDG, and it was incubated for an average of 62 minutes. The amount of injected radioactivity was routinely measured by quantification of the radioactivity of the syringe before and after injection. Patients were scanned in a supine position from the skull base to midthigh on a flat table with a head and neck acquisition separate from the body acquisition. All patients were scanned using a dedicated head and neck protocol.

The dedicated head and neck CT studies were helically acquired (120 kV[peak], gantry rotation time = 0.5 seconds, kVp = 120, auto milliamperage, minimum = 299 mA, maximum = 440 mA, noise index = 11, helical pitch factor = 0.937:1, scan FOV = 30 cm, reconstructed slice thickness = 1.25 mm, image matrix =  $512 \times 512$ ) extending from the skull base to thoracic inlet following a 60-second delay after intravenous contrast injection (60 mL of ioversol, Optiray 350, Mallinckrodt, St. Louis, Missouri; or iopamidol, Isovue 370, Bracco, Princeton, New Jersey). The images were reviewed in soft-tissue algorithms. The dedicated head and neck PET scans were obtained using 2D imaging with emission scans lasting between 5 and 6 minutes, and an FOV of 30 cm. The matrix size was  $128 \times 128$ , and slice thickness was 3.3 mm.

### **Image Segmentation and Texture Analysis on CT**

Multiple lymph nodes (up to 5 per patient, selected on the basis of a maximum size of  $>1$  cm) were analyzed for CT texture analysis and FDG uptake. Each lymph node was manually contoured by a neuroradiologist with 10 years of experience. Segmentation of the lymph nodes was performed using OsiriX Imaging Software (<http://www.osirix-viewer.com>). The entire lymph node, including necrotic or cystic areas, was segmented for analysis. For a subanalysis, ROIs without obvious necrotic or cystic areas were also created (On-line Figure). When severe streak artifacts within the lymph node were seen, the slices with severe artifacts were excluded and only artifact-free slices were used for texture analysis. Each contoured image was imported into an in-house-developed Matlab-based (MathWorks, Natick, Massachusetts) texture analysis software.<sup>24,25</sup> We discuss the extraneous math behind each texture feature in detail in a subsequent On-line Appendix.<sup>24,26–31</sup> In total, 41 texture features, including 12 histogram features, 5 gray-level co-occurrence matrix (GLCM) features, 11 gray-level run-length (GLRL) features, 4 gray-level gradient matrix (GLGM) features, and 9 Laws features, were computed and averaged over the images per dataset. The mean value of the textural features was estimated. Both the volume and size of each lymph node were also calculated.

### **[ $^{18}\text{F}$ ] FDG-PET/CT Image Analysis**

The PET study and contrast-enhanced CT scan were viewed independently and as coregistered studies using a Vista workstation (MIM Software, Cleveland, Ohio). PET, CT, and fused PET/CT images were reviewed in the axial planes. Standard uptake value maximum (SUVmax), the maximum SUV within the tumor normalized to lean body mass from PET, was measured by drawing an ROI slightly outside each lesion corresponding to those used for texture analysis on the CT image for each patient.

### **Statistical Analysis**

We compared the 41 texture parameters, SUVmax, lymph node size, and volume: 1) the malignant nodes with benign nodes in the HIV-positive group (group 2 versus 1); 2) the malignant lymph nodes with benign nodes in the HIV-negative group (group 4 versus 3); 3) the benign lymph nodes in the HIV-positive group with benign lymph nodes in the HIV-negative group (group 1 versus 3); and 4) the malignant lymph nodes in the HIV-positive group with malignant lymph nodes in the HIV-negative group (group 2 versus 4). For each group comparison, we used the mixed linear regression model (Proc MIXED; [http://support.sas.com/documentation/cdl/en/statug/63033/HTML/default/viewer.htm#mixed\\_toc.htm](http://support.sas.com/documentation/cdl/en/statug/63033/HTML/default/viewer.htm#mixed_toc.htm)) to take into consideration data clustering using the SAS 9.3 system (SAS Institute, Cary, North Carolina). Because each patient could contribute  $>1$  lymph node, this approach allowed modeling of the variance-covariance matrix among multiple values recorded for each patient. Compound symmetry was specified for the covariance structure. To assess the potential clinical utility of texture features and nodal characteristics, we constructed receiver operating characteristic curves for repeat-measures designs to determine the performance and optimal cutoff point of each parameter in distinguishing the 2 node characterizations (for example, benign versus malignant lymph nodes in HIV-positive patients).<sup>32</sup> The point on the receiver operating characteristic curve farthest from the 45-degree reference line with the best combination of sensitivity and specificity was considered the optimum cutoff point. The area under the receiver operating characteristic curve (AUC) was used to assess the predicted validity of each parameter. The closer the AUC value is to 1.0, the more predictive the features are with respect to malignant lymph nodes. Associations of demographic and clinical characteristics with HIV-positive and HIV-negative groups were tested with the Pearson  $\chi^2$  test or the Mann-Whitney  $U$  test. Due to the relatively small sample size and exploratory nature of this study, correction for multiple comparisons was not applied, and an uncorrected  $P$  value of .05 was regarded as the statistical threshold of significance for all analyses.

### **RESULTS**

For HIV-positive patients, the median absolute CD4 counts were 473 cells/mm<sup>3</sup> (range, 172–1809 cells/mm<sup>3</sup>), and 8 of 9 patients were receiving highly active antiretroviral therapy. In the HIV-positive group, 13 (59%) lymph nodes in 6 patients were confirmed as malignant (positive for metastases), and 9 (41%) lymph nodes in 5 patients were confirmed as benign (negative for metastases). Two patients in the HIV-positive group had both malignant and benign nodes. In the HIV-negative control group, 22 (36%) lymph nodes in 13 patients were confirmed as malignant (positive for metastases), and 39 (66%) lymph nodes in 20 pa-



**Table 1: Patient demographics and tumor characteristics of patients with head and neck cancer<sup>a</sup>**

Characteristic	HIV-Positive Group (n = 9)	HIV-Negative Group (n = 26)	P Value
Age (yr)			.034 <sup>b</sup>
Median (range)	48 (29–62)	59 (30–86)	
Sex			.490
Male	7 (78)	17 (65)	
Female	2 (22)	9 (35)	
HPV status (protein 16)			.283
Positive	3	12	
Negative	1	14	
Unknown	5	0	
Primary site			.169
Oropharynx	3 (33)	10 (38)	
Hypopharynx	0 (0)	1 (4)	
Larynx	1 (11)	3 (12)	
Oral cavity	3 (33)	12 (46)	
Primary unknown	1 (11)	0 (0)	
Maxilla	1 (11)	0 (0)	
T-Stage			.444
T0	1 (11)	0 (0)	
T1	1 (11)	7 (27)	
T2	3 (33)	9 (35)	
T3	1 (11)	2 (8)	
T4	3 (33)	8 (30)	

**Note:**—HPV indicates human papillomavirus.

<sup>a</sup> Data are presented as number of patients with percentages in parentheses unless otherwise noted.

<sup>b</sup> Indicates a significant difference by the Pearson  $\chi^2$  or Mann-Whitney *U* test ( $P < .05$ ).

tients were confirmed as benign (negative for metastases). Ten patients in the HIV-negative group had both malignant and benign nodes. Complete patient demographics and tumor characteristics are described in Table 1. The primary site and T-stage were not significantly different between the HIV-positive and HIV-negative groups.

### **Analysis between Lymph Node Characterization in HIV-Positive and HIV-Negative Patients with HNSCC**

**HIV-Positive Patient Group.** The results of the [<sup>18</sup>F] FDG-PET/CT characteristics (SUVmax, node size, and node volume) and the 41 texture parameters differentiating lymph node characterization in HIV-positive patients with head and neck squamous cell carcinoma (group 1 versus 2) are shown in Table 2 (for selected parameters) and On-line Table 1 (for 41 parameters). There was a significant difference in the SUVmax (5.11 for benign nodes versus 8.56 for malignant nodes,  $P = .042$ ), node size (1.40 cm for benign nodes versus 1.89 cm for malignant nodes,  $P = .024$ ), and node volume (0.55 cm<sup>3</sup> for benign nodes versus 2.54 cm<sup>3</sup> for malignant nodes,  $P = .007$ ) between malignant and benign nodes for the HIV-positive group. For the CT texture analysis in the HIV-positive group, there were 7 histogram features, including mean ( $P = .017$ ), median ( $P = .018$ ), second SD ( $P = .017$ ), range ( $P = .017$ ), geometric mean ( $P = .032$ ), SD 5 ( $P = .018$ ), and SD 9 ( $P = .017$ ); 3 GLCM features, including contrast ( $P = .009$ ), energy ( $P = .025$ ), and homogeneity ( $P = .020$ ); and 9 GLRL features, including short-run emphasis (SRE) ( $P < .001$ ), long-run emphasis (LRE) ( $P = .001$ ), gray-level nonuniformity (GLN) ( $P = .001$ ), run-length nonuniformity (RLN) ( $P = .002$ ), run percentage (RP) ( $P = .033$ ), low gray-level run emphasis

(LGRE) ( $P = .013$ ), high gray-level run emphasis (HGRE) ( $P = .008$ ), short-run low gray-level emphasis (SRLGE) ( $P = .021$ ), and long-run high gray-level emphasis (LRHGE) ( $P = .035$ ) that demonstrated a significant difference in HIV-positive patients with either benign or malignant lymph nodes (On-line Table 1). No statistically significant differences were seen in the GLGM and Laws texture features. Among the imaging characteristics, the highest AUC to predict a malignant lymph node was 0.89, with a sensitivity of 92.3% and a specificity of 77.8% in node volume. Among the 41 texture features, the highest AUC was 0.97, with a sensitivity of 84.6% and a specificity of 100% in SRE, which is categorized as a GLRL feature (Table 2).

For the HIV-positive group, the optimal SUV cutoff was 5.50 for benign-versus-malignant nodes, and 3.98 for the HIV negative group (Tables 2 and 3). Among the 13 malignant nodes, 11 (84.6%) were correctly detected by both SUV and texture analysis (SRE); however, 2 (15.4%) false-negative findings were observed even using SUV and texture analysis (SRE). Among the 9 benign nodes, 2 (22.2%) were observed as false-positive findings on the SUV cutoff point (SUVmax = 8.1 and 7.4), whereas no false-positive findings were observed on texture analysis (SRE). Figure 2 shows a representative case of a false-positive finding on FDG-PET for benign nodes in an HIV-positive patient with HNSCC who had both benign and malignant nodes.

**HIV-Negative Patient Subgroup as Controls.** The results of the [<sup>18</sup>F] FDG-PET/CT characteristics (SUVmax, node size, and node volume) and the 41 texture parameters differentiating lymph node characterization in HIV-negative patients with head and neck squamous cell carcinoma (group 3 versus 4) are shown in Table 3 (for selected parameters) and On-line Table 2 (for 41 parameters). The node volume for the HIV-negative group (1.12 mL for benign nodes versus 3.47 mL for malignant nodes,  $P = .001$ ) and the SUVmax for the HIV-negative group (3.23 for benign nodes versus 6.44 for malignant nodes,  $P = .007$ ) showed significant differences. For the CT texture analysis, statistically significant differences among lymph node characterizations in patients with head and neck squamous cell carcinoma were seen in 5 histogram features, including mean ( $P = .022$ ), geometric mean ( $P = .020$ ), harmonic mean ( $P = .020$ ), interquartile range ( $P = .022$ ), and fourth moment ( $P = .018$ ); 3 GLCM features, including contrast ( $P = .015$ ), energy ( $P = .034$ ), and homogeneity ( $P = .029$ ); 5 GLRL features, including SRE ( $P = .036$ ), RLN ( $P = .034$ ), short-run high gray-level emphasis ( $P = .016$ ), long-run low gray-level emphasis ( $P = .006$ ), and LRHGE ( $P = .003$ ); and 9 Laws features ( $P = .024$ –.047), while there was no statistically significant difference in GLGM. The highest AUC among the 41 texture features to predict a malignant lymph node was 0.76 with the texture parameter of LRHGE (sensitivity of 54.6% and specificity of 84.6%), whereas the highest AUC among the imaging characteristics was SUVmax (AUC = 0.73, sensitivity = 63.6%, and specificity = 79.5%) (Table 3).

### **Analysis of Node Characterization among HIV Infections in Patients with HNSCC with Lymph Nodes**

**Benign Lymph Node (Negative for Metastases) Subgroup.** The results of the texture parameters differentiating HIV infections in

**Table 2: <sup>18</sup>F FDG-PET/CT characteristics and selected texture parameters differentiating lymph node characterization in patients with HIV infection (group 1 vs 2)**

Texture Parameter	Benign Nodes (n = 9)		Malignant Nodes (n = 13)		P Value <sup>a</sup>	Cutoff	AUC <sup>b</sup> (GLIMMROC)
	Mean	SD	Mean	SD			
Node characteristics							
Size (cm)	1.400	0.300	1.892	0.690	.024	<2.0	0.752
Volume (cm <sup>3</sup> )	0.547	0.363	2.535	2.218	.007	>0.76	0.889
SUVmax	5.111	1.610	8.562	3.886	.042	>5.5	0.803
Histogram							
Mean	624.4	74.6	735.3	75.2	.017	>683.3	0.872
Median	774.0	217.9	1013.1	71.2	.018	>877.8	0.872
Second SD	93.76	28.70	59.85	19.19	.017	<76.3	0.872
Range	273.7	82.9	175.4	54.5	.017	<232.7	0.863
Geometric mean	199.6	44.7	272.8	63.8	.032	>237.3	0.829
SD 5	81.9	29.4	16.8	19.2	.018	<62.89	0.872
SD 9	99.7	49.3	19.5	17.3	.017	<63.16	0.889
GLCM							
Contrast	113.1	20.2	84.1	16.9	.009	<97.7	0.889
Energy	0.036	0.019	0.081	0.047	.025	>0.047	0.812
Homogeneity	0.451	0.065	0.542	0.069	.020	>0.498	0.821
GLRL							
SRE	0.177	0.007	0.157	0.009	<.001	<0.164	0.966 <sup>c</sup>
LRE	0.197	0.010	0.173	0.012	.001	<0.186	0.957
GLN	0.183	0.009	0.160	0.011	.001	<0.172	0.949
RLN	0.196	0.010	0.173	0.012	.002	<0.184	0.932
LRHGE	224.6	51.8	300.0	68.7	.035	>261.8	0.863

**Note:**—GLIMMROC indicates generalized linear mixed model receiver operating characteristic.

<sup>a</sup>Indicates a significant difference by the mixed linear regression model (Proc MIXED) to adjust the variance-covariance matrix among multiple values recorded for each patient ( $P < .05$ ).

<sup>b</sup>Using the generalized linear mixed model (GLIMMROC).

<sup>c</sup>The highest AUC among 41 texture features.

**Table 3: <sup>18</sup>F FDG-PET/CT characteristics and selected texture parameters differentiating lymph node characterization in patients with head and neck squamous cell carcinoma without HIV infection (group 3 vs 4)**

Texture Parameter	Benign Nodes (n = 39)		Malignant Nodes (n = 22)		P Value <sup>a</sup>	Cutoff	AUC <sup>b</sup> (GLIMMROC)
	Mean	SD	Mean	SD			
Node characteristics							
Size (cm)	1.439	0.048	1.687	0.831	.079	DNC	0.643
Volume (cm <sup>3</sup> )	1.122	0.147	3.468	4.718	.001 <sup>c</sup>	>2.599	0.702
SUVmax	3.228	0.315	6.438	4.811	.007 <sup>c</sup>	>3.980	0.731
Histogram							
Mean	670.6	68.4	751.8	137.3	.022 <sup>c</sup>	>738.1	0.705
Geometric mean	225.9	50.6	297.6	124.5	.020 <sup>c</sup>	>257.5	0.667
Harmonic mean	24.12	4.21	29.57	9.42	.020 <sup>c</sup>	>25.5	0.678
IQR	1064.3	63.9	865.0	360.2	.022 <sup>c</sup>	<1017.0	0.723
Fourth moment	8.71E+10	5.74E+09	9.41E+10	1.00E+10	.018 <sup>c</sup>	>9.38E+10	0.698
GLCM							
Contrast	102.5	18.2	81.8	28.3	.015 <sup>c</sup>	<75.7	0.754
Energy	0.041	0.022	0.072	0.055	.034 <sup>c</sup>	>0.058	0.712
Homogeneity	0.475	0.056	0.541	0.104	.029 <sup>c</sup>	>0.528	0.735
GLRL							
SRE	0.164	0.011	0.154	0.019	.036 <sup>c</sup>	<0.153	0.695
RLN	0.183	0.014	0.170	0.023	.034 <sup>c</sup>	<0.172	0.698
RHGE	254.2	77.2	367.0	193.6	.016 <sup>c</sup>	>305.4	0.739
LRLGE	322.6	91.4	469.8	231.9	.006 <sup>c</sup>	>397.1	0.759
LRHGE	246.2	60.5	352.7	168.8	.003 <sup>c</sup>	>340.9	0.760 <sup>d</sup>
Laws features							
LI	1,130,272.9	280,670.9	876,676.6	413,942.2	.024 <sup>c</sup>	<911,080.5	0.722

**Note:**—DNC indicates did not converge; IQR, interquartile range; GLIMMROC, generalized linear mixed model receiver operating characteristic.

<sup>a</sup>Indicates a significant difference by the mixed linear regression model (Proc MIXED) to adjust the variance-covariance matrix among multiple values recorded for each patient ( $P < .05$ ).

<sup>b</sup>Using the generalized linear mixed model (GLIMMROC).

<sup>c</sup>Significant.

<sup>d</sup>The highest AUC among 41 texture features.

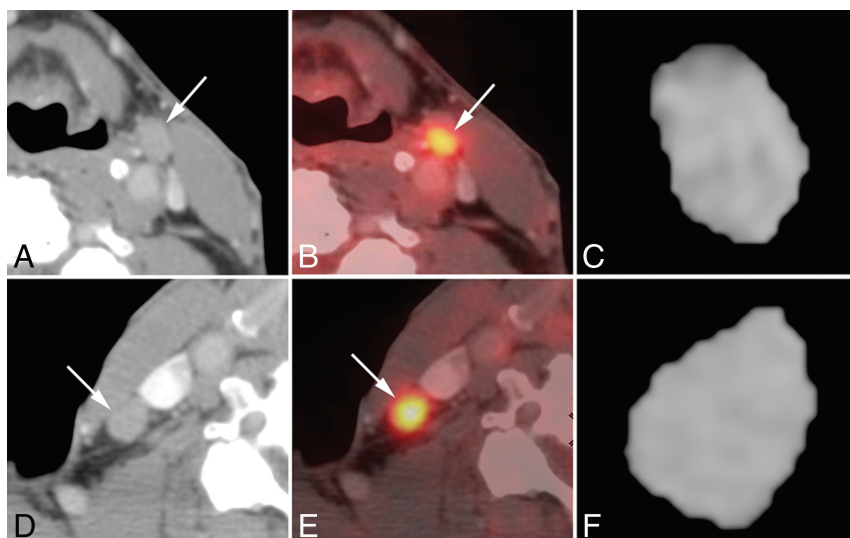


**FIG 2.** Representative case of false-positive findings on FDG-PET for benign nodes in a 74-year-old woman with unknown primary squamous cell carcinoma who had both benign and malignant nodes (HIV-positive; absolute CD4 = 473). Axial contrast-enhanced CT images (A and D), [ $^{18}\text{F}$ ] FDG-PET/CT fusion images (B and E), and corresponding axial section ROI mask-segmented lymph nodes (C and F) for pathologically benign (A–C) and malignant (D–F) lymph nodes. [ $^{18}\text{F}$ ] FDG-PET/CT shows abnormal uptake (cutoff =  $>5.5$ ) for both lymph nodes with SUVmax = 8.1 (benign, B) and 9.5 (malignant, E). However, texture features with SRE (cutoff =  $<0.164$ ) of both lymph nodes were correctly diagnosed as follows: 0.188 (benign, C) and 0.151 (malignant, F).

patients with head and neck squamous cell carcinoma with benign nodes (group 1 versus 3) are shown in On-line Table 3. For benign lymph nodes, the point estimate of the SUVmax of HIV-positive (5.11) was higher than that of HIV-negative (3.23); however, the difference among the SUVmax of HIV statuses was not statistically significant ( $P = .111$ ). No statistically significant differences were seen in the node size (1.40 cm for HIV-positive versus 1.44 cm for HIV-negative,  $P = .781$ ) and node volume ( $0.58 \text{ cm}^3$  for HIV-positive versus  $1.12 \text{ cm}^3$ ,  $P = .137$ ) between the HIV-positive and HIV-negative groups. For the CT texture analysis in benign lymph nodes, there were 5 GLRL features, SRE ( $P = .017$ ), LRE ( $P = .027$ ), GLN ( $P = .021$ ), LGRE ( $P = .044$ ), and HGRE ( $P = .012$ ), that demonstrated a significant difference with HIV-positive and HIV-negative patients. No statistically significant differences were seen in the histogram, GLCM, GLGM, and Laws texture features. Among the imaging characteristics and the 41 texture features, the highest AUC to predict HIV-infected lymph nodes was 0.87, with a sensitivity of 100% and a specificity of 84.6% in SUVmax.

**Malignant Lymph Node (Positive for Metastases) Subgroup.** The results of the texture parameters differentiating HIV infections in patients with head and neck squamous cell carcinoma with malignant nodes (group 2 versus 4) are shown in On-line Table 4. For malignant lymph nodes, there was no statistically significant differences in the SUVmax (8.56 for HIV-positive versus 6.46 for HIV-negative,  $P = .192$ ), node size (1.89 cm for HIV-positive versus 1.69 cm for HIV-negative,  $P = .186$ ), and node volume ( $2.54 \text{ cm}^3$  for HIV-positive versus  $3.47 \text{ cm}^3$ ,  $P = .409$ ) between the HIV-positive and HIV-negative groups. Of the 41 CT texture analysis parameters in malignant lymph nodes, there were no statistically significant differences in the histogram, GLCM, GLGM, GLRL, and Laws texture features.

### Subanalysis of Texture Features of Lymph Nodes without and with Exclusion of Necrotic Areas Differentiating Benign-versus-Malignant Lymph Nodes

The results of subanalysis of the lymph node characterization without and with exclusion of areas of obvious necrosis or cystic parts are shown in On-line Table 5 for patients with HIV (group 1 versus 2) and in On-line Table 6 for patients without HIV (group 3 versus 4). Even excluding the obvious necrotic parts, there was no major change in which a parameter was effective in distinguishing benign and malignant nodes. For the patients with HIV (group 1 versus 2), there were 6 histogram features ( $P = .034$ – $.045$ ), 3 GLCM features ( $P = .031$ – $.045$ ), and 4 GLRL features ( $P = .011$ – $.048$ ) that demonstrated a significant difference in HIV-positive patients with either benign or malignant lymph nodes. For the patients without HIV (group 3 versus 4), there were 3 histogram features ( $P = .032$ – $.043$ ), 2 GLCM features

( $P = .037$ – $.047$ ), and 3 GLRL features ( $P < .001$ – $.01$ ) that demonstrated a significant difference in HIV-positive patients with either benign or malignant lymph nodes. However, the AUC of the analysis, including the necrotic parts, was higher than that of the subanalysis excluding the necrotic parts for all texture parameters.

## DISCUSSION

The results of our study demonstrated that the histogram, GLCM, and GLRL CT texture parameters of the lymph nodes showed a significant difference between metastatic lymph nodes and HIV-related lymphadenopathy in patients with head and neck squamous cell carcinoma with HIV infection. CT texture features, especially space-dependent features such as GLCM and GLRL, may provide important additional information to differentiate nodal metastases from disease-specific nodal reactivity in HIV-positive patients with head and neck squamous cell carcinoma.

In our study, none of the CT textural analysis features were found to have statistically significant differences between HIV-positive and HIV-negative patients with malignant lymph nodes. The lack of a significant difference suggests almost similar texture for HNSCC metastatic nodes regardless of HIV infection status. On the other hand, benign lymph nodes showed different textures in 5 GLRL features between HIV-positive and HIV-negative lymph nodes. HIV-positive patients often have lymph node enlargement consistent with AIDS-associated reactive adenopathy, and HIV viral loads may also be associated with viral infection, including human papillomavirus and Epstein-Barr virus, which are well-known etiologies of HNSCC.<sup>6,8</sup> Therefore, the texture features may potentially reflect a different degree of uniformity due to inflammation or viral infection within the lymph nodes along both long and short matrix runs. Space-dependent texture

features such as GLRL on CT images could demonstrate significant differences in benign lymph nodes in HIV-positive patients with head and neck squamous cell carcinoma, which may have the potential to prove morphologic feature differences among disease-specific nodal reactivity in HIV-positive patients with head and neck squamous cell carcinoma.

CT texture analysis is a postprocessing technique and a new addition to the image-analysis armamentarium that extracts information native to image data that is not apparent on visual inspection of images. CT texture analysis has started to be investigated for its ability to predict lymph node metastasis in patients with lung cancer.<sup>21,33</sup> In our study, for assessment of metastatic lymph nodes in HIV-negative patients, some histogram and GLRL texture features may be associated with nodal metastasis in patients with head and neck squamous cell carcinoma. However, the predictions of malignant nodes using texture analysis were almost similar to SUV values in HIV-negative patients. Further testing using a larger sample size is needed to validate the performance of the predictive model.

Immunosuppression predisposes HIV-infected patients to a number of opportunistic infections; therefore, special care must be taken in evaluating [<sup>18</sup>F] FDG-PET/CT. Benign hypermetabolic foci are common, especially in the context of high levels of HIV viremia (low CD4 counts) and can lead to false-positive interpretations of metastasis using only the SUV cutoff point.<sup>16,18,34</sup> In past years, other quantitative approaches, including metabolic tumor volume and total lesion glycolysis for [<sup>18</sup>F] FDG-PET evaluations, have been investigated for differentiation of HIV-associated lymphoma from HIV-associated reactive adenopathy.<sup>35,36</sup> CT texture features can also be obtained from the same [<sup>18</sup>F] FDG-PET/CT study. The combination model based on these quantitative PET metabolic metrics, CT texture parameters, and clinical parameters may need to be further evaluated in a future study for patients with head and neck squamous cell carcinoma.

There are several limitations associated with the small sample size in this study. This study included only a small number of HIV-infected patients with head and neck squamous cell carcinoma, and there were imbalances among the different groups. The statistical analysis was potentially limited in that the more reasonable analyses, including multiple-comparison correction, could not be conducted. The small sample size could also potentially mask the weak differences. In addition, for the HIV-positive group, there is a wide range of absolute CD4 cell counts, and a subset of patients were receiving highly active antiretroviral therapy. These distributions have significant implications for mounting an immune reaction and therefore potentially for the texture features of lymph nodes. Therefore, detailed analyses using stratification based on CD4 counts and administration of therapeutic regimens considering the influence of the status of HIV are desirable. These problems could be solved in future studies with larger sample sizes.

## CONCLUSIONS

Histogram, GLCM, and GLRL CT texture parameters of the lymph nodes are associated with nodal metastasis in patients with head and neck squamous cell carcinoma with HIV infection. Although further testing using a larger sample size is needed to val-

idate the performance, CT texture analysis may be useful as a noninvasive method for obtaining additional quantitative information to differentiate nodal metastases from disease-specific nodal reactivity in HIV-positive patients with head and neck squamous cell carcinoma.

Disclosures: Hirofumi Kuno—UNRELATED: Grants/Grants Pending: Grant-in-Aid for Young Scientists KAKEN (#18K15573). Osamu Sakai—UNRELATED: Consultancy: Boston Imaging Core Lab.

## REFERENCES

- Antiretroviral Therapy Cohort Collaboration. Life expectancy of individuals on combination antiretroviral therapy in high-income countries: a collaborative analysis of 14 cohort studies. *Lancet* 2008; 372:293–99 CrossRef Medline
- Bonnet F, Burty C, Lewden C, et al. Changes in cancer mortality among HIV-infected patients: the Mortalité 2005 Survey. *Clin Infect Dis* 2009;48:633–39 CrossRef Medline
- Coghill AE, Shiels MS, Suneja G, et al. Elevated cancer-specific mortality among HIV-infected patients in the United States. *J Clin Oncol* 2015;33:2376–83 CrossRef Medline
- Mourad WF, Hu KS, Shasha D, et al. Long-term outcome of seropositive HIV patients with head and neck squamous cell carcinoma treated with radiation therapy and chemotherapy. *Anticancer Res* 2013;33:5511–16 Medline
- Powles T, Robinson D, Stebbing J, et al. Highly active antiretroviral therapy and the incidence of non-AIDS-defining cancers in people with HIV infection. *J Clin Oncol* 2009;27:884–90 CrossRef Medline
- Beachler DC, Sugar EA, Margolick JB, et al. Risk factors for acquisition and clearance of oral human papillomavirus infection among HIV-infected and HIV-uninfected adults. *Am J Epidemiol* 2015;181: 40–53 CrossRef Medline
- Frisch M, Biggar RJ, Engels EA, et al. Association of cancer with AIDS-related immunosuppression in adults. *JAMA* 2001;285: 1736–45 CrossRef Medline
- McLemore MS, Haigentz M Jr, Smith RV, et al. Head and neck squamous cell carcinomas in HIV-positive patients: a preliminary investigation of viral associations. *Head Neck Pathol* 2010;4:97–105 CrossRef Medline
- Spano JP, Costagliola D, Katlama C, et al. AIDS-related malignancies: state of the art and therapeutic challenges. *J Clin Oncol* 2008;26:4834–42 CrossRef Medline
- D'Souza G, Carey TE, William WN Jr, et al. Epidemiology of head and neck squamous cell cancer among HIV-infected patients. *J Acquir Immune Defic Syndr* 2014;65:603–10 CrossRef Medline
- Olsen WL, Jeffrey RB Jr, Sooy CD, et al. Lesions of the head and neck in patients with AIDS: CT and MR findings. *AJR Am J Roentgenol* 1988;151:785–90 CrossRef Medline
- Holliday RA, Cohen WA, Schinella RA, et al. Benign lymphoepithelial parotid cysts and hyperplastic cervical adenopathy in AIDS-risk patients: a new CT appearance. *Radiology* 1988;168:439–41 CrossRef Medline
- Quon A, Fischbein NJ, McDougall IR, et al. Clinical role of <sup>18</sup>F-FDG PET/CT in the management of squamous cell carcinoma of the head and neck and thyroid carcinoma. *J Nucl Med* 2007;48(Suppl 1):58S–67S Medline
- Kyzas PA, Evangelou E, Denaxa-Kyza D, et al. <sup>18</sup>F-fluorodeoxyglucose positron emission tomography to evaluate cervical node metastases in patients with head and neck squamous cell carcinoma: a meta-analysis. *J Natl Cancer Inst* 2008;100:712–20 CrossRef Medline
- Gupta T, Master Z, Kannan S, et al. Diagnostic performance of post-treatment FDG PET or FDG PET/CT imaging in head and neck cancer: a systematic review and meta-analysis. *Eur J Nucl Med Mol Imaging* 2011;38:2083–95 CrossRef Medline
- Davison JM, Subramaniam RM, Surasi DS, et al. FDG PET/CT in patients with HIV. *AJR Am J Roentgenol* 2011;197:284–94 CrossRef Medline



17. Sathekge M, Maes A, Kgomo M, et al. **Fluorodeoxyglucose uptake by lymph nodes of HIV patients is inversely related to CD4 cell count.** *Nucl Med Commun* 2010;31:137–40 [CrossRef Medline](#)
18. Sathekge M, Maes A, Van de Wiele C. **FDG-PET imaging in HIV infection and tuberculosis.** *Semin Nucl Med* 2013;43:349–66 [CrossRef Medline](#)
19. Frankel SS, Tenner-Racz K, Racz P, et al. **Active replication of HIV-1 at the lymphoepithelial surface of the tonsil.** *Am J Pathol* 1997;151:89–96 [Medline](#)
20. Goldenberg D, Sciubba J, Koch WM. **Cystic metastasis from head and neck squamous cell cancer: a distinct disease variant?** *Head Neck* 2006;28:633–38 [CrossRef Medline](#)
21. Bayanati H, Thornhill RE, Souza CA, et al. **Quantitative CT texture and shape analysis: can it differentiate benign and malignant mediastinal lymph nodes in patients with primary lung cancer?** *Eur Radiol* 2015;25:480–87 [CrossRef Medline](#)
22. Huang YQ, Liang CH, He L, et al. **Development and validation of a radiomics nomogram for preoperative prediction of lymph node metastasis in colorectal cancer.** *J Clin Oncol* 2016;34:2157–64 [CrossRef Medline](#)
23. Knogler T, El-Rabadi K, Weber M, et al. **Three-dimensional texture analysis of contrast enhanced CT images for treatment response assessment in Hodgkin lymphoma: comparison with F-18-FDG PET.** *Med Phys* 2014;41:121904 [CrossRef Medline](#)
24. Buch K, Fujita A, Li B, et al. **Using texture analysis to determine human papillomavirus status of oropharyngeal squamous cell carcinomas on CT.** *AJNR Am J Neuroradiol* 2015;36:1343–48 [CrossRef Medline](#)
25. Fujita A, Buch K, Li B, et al. **Difference between HPV-positive and HPV-negative non-oropharyngeal head and neck cancer: texture analysis features on CT.** *J Comput Assist Tomogr* 2016;40:43–47 [CrossRef Medline](#)
26. Haralick RM, Shanmugam K, Dinstein IH. **Textural features for image classification.** *IEEE Transactions on Systems, Man and Cybernetics* 1973;SMC-3:610–21 [CrossRef Medline](#)
27. Laws KI. *Textured Image Segmentation* [dissertation and thesis]. Los Angeles: University of Southern California; 1980
28. Tang X. **Texture information in run-length matrices.** *IEEE Trans Image Process* 1998;7:1602–09 [CrossRef Medline](#)
29. Castellano G, Bonilha L, Li LM, et al. **Texture analysis of medical images.** *Clin Radiol* 2004;59:1061–69 [CrossRef Medline](#)
30. Yu H, Buch K, Li B, et al. **Utility of texture analysis for quantifying hepatic fibrosis on proton density MRI.** *J Magn Reson Imaging* 2015;42:1259–65 [CrossRef Medline](#)
31. Li B, Jara H, Yu H, et al. **Enhanced Laws textures: a potential MRI surrogate marker of hepatic fibrosis in a murine model.** *Magn Reson Imaging* 2017;37:33–40 [CrossRef Medline](#)
32. Liu H, Wu T. **Estimating the area under a receiver operating characteristic (ROC) curve for repeated measures design.** *Journal of Statistical Software* 2003;8:1–18 [CrossRef](#)
33. Pham TD, Watanabe Y, Higuchi M, et al. **Texture analysis and synthesis of malignant and benign mediastinal lymph nodes in patients with lung cancer on computed tomography.** *Sci Rep* 2017;7:43209 [CrossRef Medline](#)
34. Brust D, Polis M, Davey R, et al. **Fluorodeoxyglucose imaging in healthy subjects with HIV infection: impact of disease stage and therapy on pattern of nodal activation.** *AIDS* 2006;20:985–93 [CrossRef Medline](#)
35. Mhlanga JC, Durand D, Tsai HL, et al. **Differentiation of HIV-associated lymphoma from HIV-associated reactive adenopathy using quantitative FDG PET and symmetry.** *Eur J Nucl Med Mol Imaging* 2014;41:596–604 [CrossRef Medline](#)
36. Lawal IO, Nyakale NE, Harry LM, et al. **The role of F-18 FDG PET/CT in evaluating the impact of HIV infection on tumor burden and therapy outcome in patients with Hodgkin lymphoma.** *Eur J Nucl Med Mol Imaging* 2017;44:2025–33 [CrossRef Medline](#)